POLITECNICO
MILANO 1863

SCUOLA DI INGEGNERIA INDUSTRIALE
E DELL'INFORMAZIONE

Executive Summary of the Thesis

THEORETICAL AND EXPERIMENTAL ANALYSIS OF FREQUENCY MODULATED MEMS ACCELEROMETERS WITH INNOVATIVE ELECTRODES TOPOLOGY

Laurea Magistrale in Electronics Engineering - Ingegneria Elettronica

Author: Luca Pileri

Advisor: Prof. Giacomo Langfeleder

Co-advisor: Christian Padovani

Academic year: 2022-2023

1. Introduction

Among all topologies in literature, the frequency modulation accelerometer based on the time-switched concept (TSFM) represents the most promising one, resolving the zero-g offset thermal drift which characterizes both the amplitude modulation (AM) and frequency modulation (FM) based on other concepts. The TSFM consists in a double mass rotor, which is kept in oscillation in anti-phase at a frequency f_{ap} by a control circuit. In response to an external acceleration, two sets of parallel plates, operating in complementary mode, modulates f_{ap} from which the acceleration information is retrieved. However, the adoption of parallel electrodes introduce the trade-off between large displacement, required for noise performance, and limited rotor motion, imposed by pull-in.

The present Thesis work proposes two alternative electrode topologies to overcome the TSFM limitations. The first solution consists in the implementation of shaped comb finger (SCF) as tuning electrodes, in substitution to the parallel plate topology. The SCF extends the rotor travel range thanks to the mitigation of the pull-in effect. The topology will be studied in detail, starting from the definition of a geometrical model of the electrodes at which follows the mechanical and electronics design of an accelerometer. The MEMS performances will be evaluated in a Simulink model, where the theoretical sensitivity and resolution are simulated. The second solution is based on a TSFM architecture with a piezo-resistive readout based on nano-gauges. The experimental test on the device extracts information relative to noise and scale factor performances, underlining the benefits and drawbacks in comparison to the accelerometer on the market.

2. Shaped comb finger

A comb-drive electrode consists of interspersed moving and fixed conductive fingers. When a bias voltage is applied across the combs, the electrodes generates an electrostatic force whose magnitude depends on the applied voltage as well as the geometry of the fingers. For rectangular comb fingers, the geometry results in a constant gap between fixed and moving fingers. The shaped comb finger represents a way to vary the gap along the rotor travel range, generating

an electrostatic force which depends on the designed finger profile.

2.1. Mathematical evaluation of the scale factor

The investigation focuses on the research of a suitable comb profile which emphasizes the quadratic component of the electrostatic force to match the scale factor obtained with parallel plate implementation. For this reason, the input to output relation is generalized assuming an undefined tuning electrodes. The calculation are carried out basing on the TSFM model presented by Padovani et. al. [4], which is reported in Figure 1.

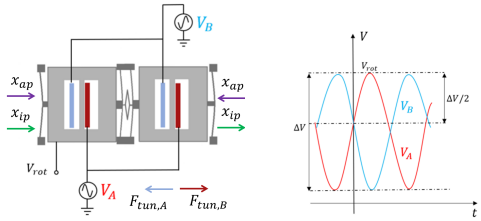

(a) Motion notation. (b) Tuning.

Figure 1: TSFM model [4].

The electrostatic force of N tuning electrodes is schematized by a second order polynomial equation:

$$F_{elec}(x) = (QT \cdot x^2 + LT \cdot x + CT) \cdot N \cdot \Delta V_{tun}^2 \tag{1}$$

where QT is the quadratic term, LT is the linear term, and CT is the constant term of the electrostatic force model. The two set of electrodes will be driven by two sinusoidal voltage signals, phase-out of 180° between each other, with an amplitude of ΔV at the switching frequency f_{sw}. From the equation (1) the anti-phase component of the tuning force is extracted, resulting in:

$$\begin{aligned} F_{tun}^{AP} = \frac{N \cdot \Delta V^2}{2} [(1 + \sin^2(\omega_{sw} t)) \cdot LT \\ -4 \cdot QT \cdot x_{ip} \sin(\omega_{sw} t)] \cdot x_{ap} \\ = k_{el,ap}(t) \cdot x_{ap}. \end{aligned} \tag{2}$$

The main components of the anti-phase tuning force is the first harmonic at ω_{sw}, which carries the information about the acceleration, i.e. x_{ip}. The tuning electrostatic force induces a softening effect on the anti-phase resonant mode, modulating the f_{ap}. A demodulation step, consisting in the multiplication of f_{ap} by a sine at f_{sw}, converts the accelerometer information into a DC signal. The demodulated frequency is filtered to remove the non-DC components, obtaining the sensitivity equation:

$$\frac{\Delta f_{AP}}{\Delta a} = \frac{1}{2} \cdot \frac{1}{2\pi^2} \cdot (2QT \cdot N) \cdot \frac{1}{k_{IP}} \cdot \frac{1}{f_{AP,0}} \tag{3}$$

in which the factor 1/2 comes from the demodulation step. It is interesting to evidence that the only contribution that remains in the scale factor, from the initial electrostatic force equation (1), is the quadratic term (QT).
From the comparison between (3) and the scale factor of the TSFM with tuning PP, the amount of needed electrodes to match the two sensitivities is extracted:

$$N = \frac{3 L_{PP} H \epsilon_0}{2 g^4 QT} \tag{4}$$

where L_{PP} is the length of a parallel plate, H is the process height, and g the initial gap of the tuning plates. The number has to be referred to a single tuning side per mass.

2.2. Profile design

The shaped comb finger electrostatic is simplified to expressed the geometrical dependence of the force on the SCF profile. A relationship between force and gap profiles in a SCF was discussed by Jensen at al. studies [1]. The same model is used in this study: considering $f_1(x)$ and $f_2(x)$, respectively, the profile functions of the moving and fixed finger, the electrostatic force relation of a single SCF corresponds to

$$F_{SCF}(x_{eng}) = \frac{1}{2} \frac{\epsilon_0 H V^2}{g(x_{eng})}. \tag{5}$$

where the gap between comb fingers coincides with $g(x) = f_1(x) - f_2(x)$, and x_{eng} is the engagement term. Basing on the equation (5), the gap is designed to achieve an electrostatic force which approximates the general equation (1). The choice ends up in a profile function inversely proportional to a second order equation of the engagement (x):

$$f(x) = \frac{A}{B + C \cdot x + x^2} \tag{6}$$

where parameters A, B, and C are set by the geometric constraints. Designing both the comb

fingers with the profile equation (6), the gap between rotor and stator coincides with the double of the shape equation (6). Substituting the relation (6) in (1), the obtained result is a second order polynomial, suitable for an implementation as tuning electrodes for the TSFM application. The half pitch structure, i.e. comprehending just two SCF halves, is simulated as a 2D Comsol model where only the air between rotor and stator is considered to save computational cost. An electrostatic stationary study were accomplished using the boundary element method (BEM), retrieving the force characteristic of the SCF. The comb finger geometry is presented in 2 where the main geometrical parameters are indicated.

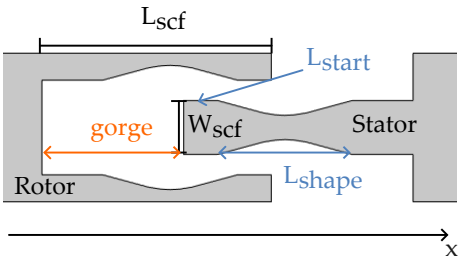

Figure 2: Full pitch geometry of a double SCF.

The design optimization is accomplished through the analysis of each geometric parameter on the quadratic term, retrieving a configuration which minimizes the product between area occupation and required shaped comb finger. The optimization leads to the electrostatic force presented in Figure 3, whose geometrical parameters and performances are reported in table 1. The designed shaped

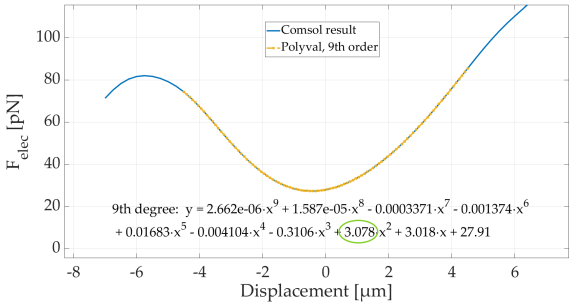

Figure 3: Relation between electrostatic force and displacement for half SCFd pitch.

comb finger allows the increasing of the rotor travel range to ±4.5 µm, extending the limited displacement constraint of the TSFM PP, equal

Shape parameter	Value
Pitch	11 µm
Mass single SCF	3.828 pKg
$TQ(half\ pitch)$	3.078 N/m^2
N_{scf}	565
gap_0	1.5 µm

Table 1: Summary of parameters chosen to optimized the SCFd design.

to 400 nm.
The shaped comb finger topology is also tested in a condition of maximum positive and negative overetch, i.e. in presence of process damage which introduces a geometrical variation of ±0.2 µm. The simulations will be useful in the scale factor evaluation.

2.3. Mechanical design

After the shaped comb finger definition, the mechanical structure of an in-plane accelerometer was defined in COMSOL. The 2D top view of the layout is presented in figure 4.

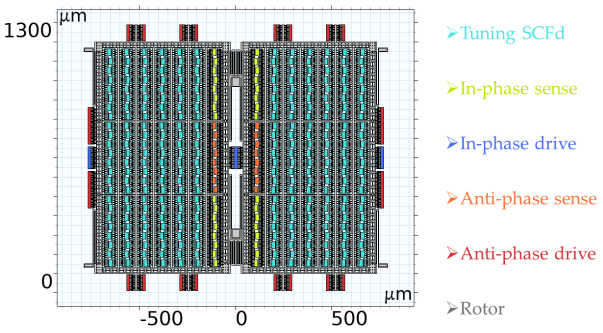

Figure 4: COMSOL layout of the TSFM with SCFd tuning electrodes.

The new achievable travel range allows the lowering of in-phase and anti-phase modes, chosen to be 4 kHz and 24.9 kHz, respectively. However, the increased mass weight of the accelerometer, due to SCF implementation, represents the main challenge of the design. A heavy mass brings issues related both to the scale factor and to the rejection of out-of-plane spurious mode. The solution relies on the application of a truss to the external frame of the rotor, which lightens the structure without softening the electrode shuttle stiffness. The truss implementation is shown in figure 5, which is characterized by a beam width

W_{gir} of 3 µm for a W_m frame width of 30 µm.

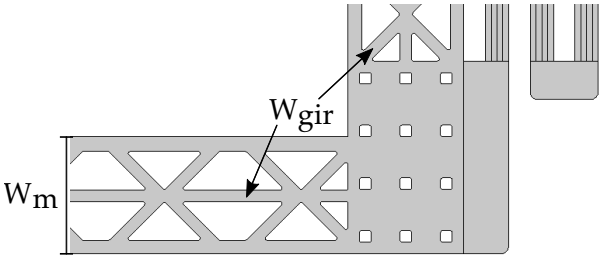

Figure 5: Girder and holes.

In addiction to the truss, two horizontals beams divide each mass in three sections: the division has benefit in terms of out-of-plane modes rejection. Moreover, this approach also allows to separate the AP drive detection from the IP one, improving the feedthrough capacitance compensation and reducing the number of C2V required for the readout circuit. The obtained structures show the first spurious mode at 27.24 kHz, at a frequency distance of 3 kHz from the f_{ap}, as it can be evidenced in the figures 6.

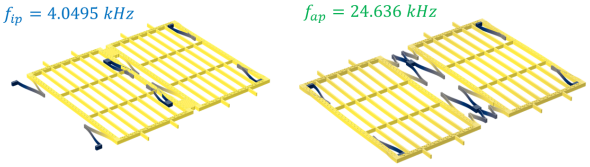

(a) In-phase and anti-phase modes.

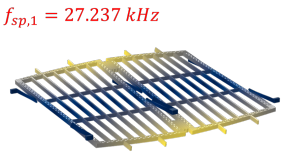

(b) Spurious modes.

Figure 6: System modes.

The mechanical analysis also estimates the impact of the overetch on the mechanical and electrostatic performances of the device. The conducted eigenvalue studies, in the worst overetch conditions, still show a rejection of the out-of-plane spurious modes, proving the strength of the designed device.

3. Simulink circuit analysis

The control electronic of the TSFM accelerometer represents a key aspect in the device definition: the sensor system requires the oscillation of the rotor in its anti-phase mode, in order to acquired the acceleration through the f_{ap} variations. An oscillation loop fulfill the requirement: it is a positive feedback circuit, which keeps the structure oscillation in anti-phase at a fixed x_{ap} displacement amplitude. The loop is provided with an AGC circuit, whose role is to adjust the loop gain to stabilize the oscillation loop at a target amplitude $x_{ap,target}$. The circuit schematic implementation is accomplished in a mathematical environment (Simulink), alongside a model for the tuning electrodes and rotor mechanics. The Simulink model is used to simulate the device performances, also taking into account the non-linear effect of the tuning electrodes.

3.1. Displacement consideration

First of all, the correct operation of the device in the rotor travel range is verified. Aiming to a total displacement at 100g of 4.5 µm, the device has to satisfies the following requirements:

- 2 µm from AP motion. It corresponds to $x_{ap,target}$;
- 1 µm for the in-phase tuning. Indeed, the electrostatic force of the tuning electrodes has an in-phase component which adds an oscillating contribution to the IP motion;
- 1.51 µm for the linear displacement induced by acceleration.

3.2. Q_{ip} compensation

Alongside the oscillation circuit, a compensation loop is designed for this device, improving the interference rejection properties of the MEMS and mitigating the ringing effect of the IP response. The compensation loop is based on the same concept of a negative force feedback circuit. The Simulink model takes in consideration an estimated $Q_{ip} = 600$, corresponding to a decay time of $\tau = 47.7$ ms, and computes a simulation with an abrupt acceleration of 20g. The result shows a reduction of the ringing effect to 0.2 ms.

3.3. Sensitivity and linearity

To retrieve the scale factor, a Simulink simulation is performed, obtaining the sensitivity in a range of $\pm 100g$. The linearity is defined by the relative error between real SF and its linear approximation. The results, presented in figure 7, show a simulated sensitivity of 0.88 Hz/g in lights of a sub 1% linear error in a range of $\pm 47g$.

Two overetched simulations, both for negative

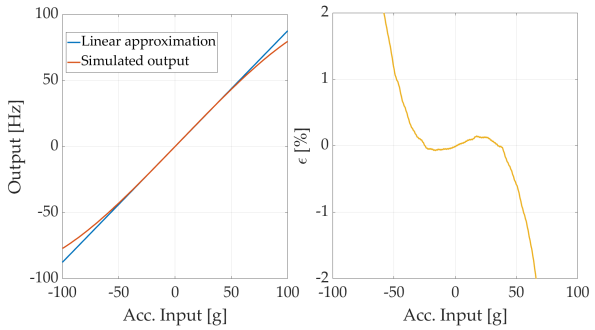

Figure 7: Simulation of the scale factor and linearity of the accelerometer, performed in the Simulink environment.

and positive OE value, are also performed, showing a quasi unaltered scale factor in lights of a relevant linearity variation.

3.4. Noise evaluation

The Simulink model is now used to extract the resolution performance of the device. The simulation is accomplished in absence of input signal, considering the white noise component related to the OPAMP of the Charge Amplifier (CA), the feedback resistance of the CA, and the mechanical noise of the rotor. Other contribution are considered negligible because mitigated by the gain stage. Regarding the tuning electrodes noise, three different condition are considered:

- no noise component in the tuning generator;
- white noise component with a PSD of $(10\ \mu V/\sqrt{Hz})^2$;
- a flicker noise, generated starting from a white noise source with $P_w = (60\ \mu V/\sqrt{Hz})^2$.

Each input noise spectra is reported in figure 8, whose obtained noise floor at 100 Hz are, respectively, 1 $\mu g/\sqrt{Hz}$, 22 $\mu g/\sqrt{Hz}$, and 93 $\mu g/\sqrt{Hz}$.

3.5. Conclusion of SCF

The SCF implementation has showed promising results in terms of the linearity and phase noise performances. Indeed, the work of Marra at al. [3] shows a repeatable sub-1% input range of 32 g alongside a 100 $\mu g/\sqrt{Hz}$ noise floor. These results are theoretically reached and overcomed by the TSFM with SCF tuning electrodes.

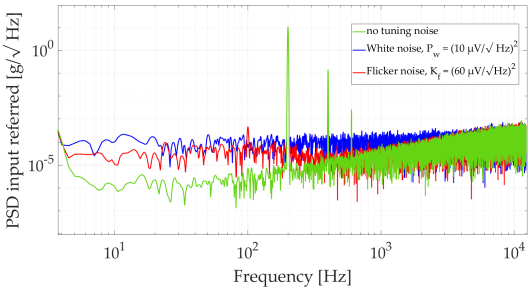

Figure 8: Input referred noise comparison between different tuning noise sources.

4. TSFM with PZT electrodes

This proposed solution relies on the improvement of the noise performances through the increased available signal in the AP readout circuit. The PZT electrodes accomplishes the result, improving the V/x transduction factor without the area occupation cost. Moreover, the Wheatstone bridge circuit, necessary to convert the resistance variation into a voltage signal, is unaffected by parasitic capacitance contributions.

4.1. Electronics

In a board with discrete components, the implementation of the main control circuits for the working operation of the TSFM is accomplished. The electronics design comprehends:

- an oscillation loop for the actuation of the rotor in anti-phase;
- an AGC circuit for the stabilization of the x_{ap} amplitudes;
- a frequency reader to convert the sinusoidal anti-phase signal into a squared one.

The tested oscillation circuit shows an open loop gain which differs from the theoretical one: the resonance peak is moved from the expected 55 kHz to 51.11 kHz due to the process variation influence on the modal springs. Moreover, the experimental DC open loop gain is higher than the theoretical one, meaning a reduction of the nominal gap in the driving CF due to the process step.

4.2. Noise

Both the accelerometers in the package are experimentally characterized in absence of signal, extracting the noise information. Figure 9 illustrates the power mean of ten acquisitions.

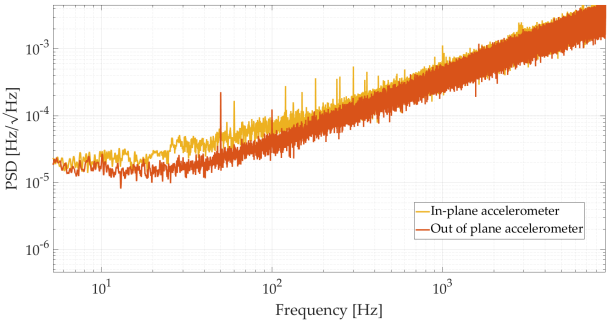

Figure 9: Out-of-plane accelerometer output spectrum without the tuning.

Both the in-plane and out-of-plane accelerometers show promising noise performances, respectively of 75 µHz/$\sqrt{Hz}$ and 38.9 µHz/$\sqrt{Hz}$ at 100 Hz. The measured resolutions is not achievable by other MEMS accelerometers, in particular for the out-of-plane detection for which the best result is represented by the amplitude modulation OOP accelerometer in literature [2], showing a resolution of 76 µHz/$\sqrt{Hz}$.

4.3. Scale factor and linearity

For the scale factor evaluation, the board is placed on a table rate, used to induce on the in-plane accelerometer an unitary g acceleration at f_{rate}. The sensitivity is quantified looking at the sinusoidal amplitude of the demodulated and filter f_{ap} signal circulating in the oscillation loop. The resulting filtered frequency is illustrated in Figure 10. The plot shows a sensitivity

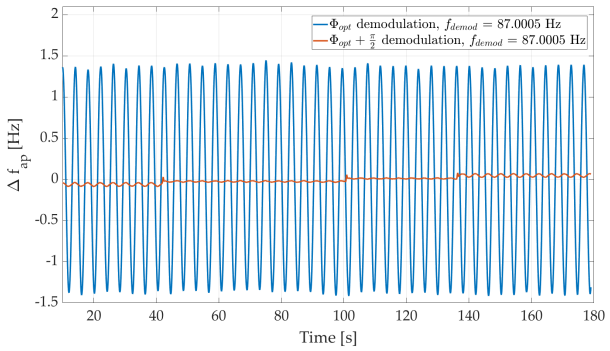

Figure 10: Demodulated and filtered output frequency acquired from the FPGA.

of 1.54 Hz/g, reaching the SF performances of other tested TSFM present in literature. However, the analysis also evidence a spurious tone in the scale factor: its appearance is related to the third harmonic components of the output frequency, which must be attenuated using a filter before the demodulation step.

5. Conclusion

In this thesis work, the SCF geometry was defined in order to reach, theoretically, the same scale factor of the architecture with PP. The mechanical and electronics implementation allows the prediction of the theoretical performances of the device, confirming the performance improvements.
The electronics of the TSFM with PZT drive detection was designed in order to characterize the device. From the experimental results, the scale factor and noise performances was measured, verifying the benefits of the implementation.

References

[1] B.D. Jensen, S. Mutlu, S. Miller, K. Kurabayashi, and J.J. Allen. Shaped comb fingers for tailored electromechanical restoring force. *Journal of Microelectromechanical Systems*, 12(3):373–383, 2003.

[2] Y. Jeong, A. Daruwalla, H. Wen, and F. Ayazi. An out-of-plane "hinge-shaped" nano-gap accelerometer with high sensitivity and wide bandwidth. In *2017 19th International Conference on Solid-State Sensors, Actuators and Microsystems (TRANSDUCERS)*, pages 2131–2134, 2017.

[3] Cristiano Rocco Marra, Alessandro Tocchio, Francesco Rizzini, and Giacomo Langfelder. Solving fsr versus offset-drift trade-offs with three-axis time-switched fm mems accelerometer. *Journal of Microelectromechanical Systems*, 27(5):790–799, 2018.

[4] Christian Padovani, Riccardo Nastri, Leonardo Gaffuri Pagani, Paolo Frigerio, Francesco Rizzini, and Giacomo Langfelder. Continuous mode-reversal fm accelerometer with 60-g fsr, 10-µg/k drift, and vre rejection. *Journal of Microelectromechanical Systems*, 31(6):857–866, 2022.